

Determination of the Metal Ion Separation and Energies of the Three Lowest Electronic States of Dimanganese(II,II) Complexes and Enzymes: Catalase and Liver Arginase[†]

S. V. Khangulov,^{‡,§} P. J. Pessiki,[§] V. V. Barynin,^{||} D. E. Ash,[⊥] and G. C. Dismukes^{*,§}

Henry H. Hoyt Laboratory, Department of Chemistry, Princeton University, Princeton, New Jersey 08544, Institute of Crystallography, Russian Academy of Sciences, Moscow, Russia, and Department of Biochemistry, Temple University School of Medicine, Philadelphia, Pennsylvania 19140

Received September 22, 1994[®]

ABSTRACT: The dimanganese(II,II) catalase from *Thermus thermophilus*, MnCat(II,II), arginase from rat liver, Arg(II,II), and several dimanganese(II,II) compounds, LMn₂XY₂, which are functional catalase mimics, all possess a pair of coupled Mn(II) ions in their catalytic sites. For each of these, we have measured by EPR spectroscopy the relative energies separating the three lowest electronic states (singlet, triplet, and quintet), described a general method for extracting the individual spectra for these states by multicomponent analysis, and determined the Mn–Mn separation. The triplet–singlet and quintet–singlet energy gaps were modeled well by fitting the temperature dependence of the EPR intensities to a Boltzmann expression for a pair of Mn(II) ions coupled by isotropic Heisenberg spin exchange ($-2JS_1S_2$). This dependence indicates diamagnetic ground states with ΔE_{10} (cm⁻¹) = $|2J|$ = 4 and 11.2 cm⁻¹ for Arg-(II,II)(+borate) and MnCat(II,II)(phosphate), respectively. This large difference in $|2J|$ reflects either a difference in the bridging ligands or, possibly, a weaker ligand field (larger ionization potential) for the Mn(II) ions in arginase. In *n*-butanol/CH₂Cl₂ the triplet–singlet energy gaps for [LMn₂(CH₃CO₂)](ClO₄)₂ (1), [LMn₂(CH₃CO₂)₃] (2), and [LMn₂Cl₃] (3), where HL = *N,N,N',N'*-tetrakis(2-methylenebenzimidazole)-1,3-diaminopropan-2-ol, are 23–24 cm⁻¹. Comparison of the Heisenberg exchange interaction constants for more than 30 dimanganese(II,II) complexes suggests a possible bridging structure of (μ -OH)(μ -carboxylate)_{1–2} for MnCat(II,II), while the 3-fold weaker coupling in Arg(II,II) suggests μ -aqua in place of μ -hydroxide. EPR spectra of both the triplet and quintet electronic states were extracted and found to exhibit zero-field splittings (ZFS) and resolved ⁵⁵Mn hyperfine splittings indicating spin-coupled Mn₂-(II,II) species. The major ZFS interaction could be attributed to the magnetic dipole–dipole interaction between the Mn(II) ions. A linear correlation is observed between the crystallographically determined Mn–Mn distance and the ZFS of the quintet state (D₂) for five dimanganese pairs for which both data sets are available. Using this correlation, the Mn–Mn distance in Arg(II,II) is predicted to be 3.36–3.57 Å for the native enzyme (multiple forms) and 3.59 Å for MnCat(II,II)(phosphate). Addition of the inhibitor borate to Arg(II,II) simplifies the ZFS, indicative of conversion to a single species with mean Mn–Mn separation of 3.50 Å. The second metal ion in dinuclear complexes possessing a shared bridging ligand has been shown to attenuate the strength of the μ -ligand field potential, as monitored by the strength of the single ion ZFS. A weakened μ -ligand field potential may play a role, for example, in promoting ionization of a proton from a manganese-bound water molecule in arginase, with the resulting hydroxide ligand being the nucleophile needed for hydrolysis of substrate.

A number of di- and tetramanganese enzymes have been discovered or characterized in the last decade which participate in various biological processes including hydrogen peroxide disproportionation (catalases) (Kono & Fridovich, 1983a,b; Barynin et al., 1986; Vainshtein et al., 1984, 1985; Barynin, 1991; Khangulov et al., 1986, 1987, 1990a–d; Waldo et al., 1992; Penner-Hahn, 1992), deoxyribonucleotide synthesis (bacterial ribonucleotide reductases) (Willing et al., 1988), L-arginine hydrolysis (arginase) (Reczkowski, 1990;

Reczkowski & Ash, 1992), energy metabolism in thiobacilli (thiosulfate-oxidizing enzyme) (Cammack et al., 1989), isomerization of 1,2-ketoalcohols such as glucose to fructose (xylose isomerase) (Carrel et al., 1989; Whitlow et al., 1991; Collyer et al., 1990), hydrolytic cleavage of RNA (RNAase domain of HIV-1 reverse transcriptase) (Davies et al., 1991), and photosynthetic oxygen production from water (water oxidase) (Dismukes & Siderer, 1981). Each of these enzymes contains a pair of ligand-bridged Mn ions at the active site or, in the case of the water oxidase, a tetranuclear Mn site (Dismukes, 1992).

Because manganese ions are paramagnetic, EPR spectroscopy can often provide information on the number of Mn ions, their distance of separation and oxidation states, the magnitudes of the Mn–Mn Heisenberg spin exchange and magnetic dipole–dipole interactions, the spin multiplicity of the lowest electronic states, and the spatial symmetry of the

[†] This research was supported by grants from the National Institutes of Health, GM-39932 and DK-45414 (to G.C.D.) and DK-44841 (to D.E.A.).

[‡] Present address: NIH, National Heart, Lung and Blood Institute, Bethesda, MD 20892.

[§] Princeton University.

^{||} Russian Academy of Sciences.

[⊥] Temple University School of Medicine.

[®] Abstract published in *Advance ACS Abstracts*, January 15, 1995.

Mn ligand field. However, EPR spectra for both proteins and synthetic complexes in the $\text{Mn}_2(\text{II,II})$ oxidation state are usually quite complex, often with several of the six low-lying electronic states (spin $S = 0, 1, \dots, 5$) contributing to the spectrum, owing to small energy separations between states. The EPR spectra of these states overlap, making separation and analysis of the ^{55}Mn hyperfine and zero-field splittings quite difficult. Here we apply the method of multicomponent analysis to obtain a deconvolution of the individual EPR spectra and assign the spin multiplicities and Boltzmann energy gaps for the two lowest excited spin states arising from the manifold of six states of $\text{Mn}_2(\text{II,II})$ compounds and proteins. We apply this methodology to the $\text{Mn}_2(\text{II,II})$ state of rat liver arginase, the catalase from *Thermus thermophilus*, and three derivatives of the model compound **1**, $[\text{LMn}_2(\text{CH}_3\text{CO}_2)](\text{ClO}_4)_2$, where $\text{HL} = N,N,N',N'$ -tetrakis(2-methylenebenzimidazole)-1,3-diaminopropan-2-ol. The resulting Heisenberg exchange constants are compared to those for a wide range of dimanganese(II,II) complexes.

It is also possible to determine the distance between the Mn(II) ions from the zero-field splitting (ZFS) parameter, D_s , that corresponds to the EPR signal from a certain spin state S . We have found that there is a good linear correlation between the crystallographically determined Mn–Mn distance and the EPR determined D_2 values for five examples for which both data sets are available. This method is most valuable in cases of disordered systems where X-ray diffraction is not applicable and where Mn EXAFS often fails to detect scattering from the neighboring Mn(II). However, Mn EXAFS is a very effective tool for characterizing Mn pairs in higher oxidation states (Waldo & Penner-Hahn, 1992; Penner-Hahn, 1992). A preliminary account of this work has been presented (Pessiki et al., 1992).

EXPERIMENTAL PROCEDURES

Synthesis and Structural Analysis. Synthesis and structural analysis of $[\text{LMn}_2(\text{CH}_3\text{CO}_2)](\text{ClO}_4)_2$ (**1**), $[\text{LMn}_2(\text{CH}_3\text{CO}_2)_3]$ (**2**), and $[\text{LMn}_2\text{Cl}_3]$ (**3**) have been reported elsewhere (Pessiki et al., 1993; Mathur et al., 1987). The structure of **1** was determined by X-ray crystallography.

Manganese Catalase. Mn-catalase was purified as described previously and stored at 5 °C as a fine crystalline precipitate in half-saturated ammonium sulfate solution (Barynin & Grebenko, 1986). Preparations of reduced catalase were obtained by dialysis against 100 μM $(\text{NH}_2\text{OH})_2\text{H}_2\text{SO}_4$ for 1 h. To remove excess reductant (hydroxylamine) and obtain the phosphate derivatives, $\text{MnCat}(\text{II,II})\text{-(Ph)}$, the reduced enzyme, was dialyzed against 100 mM potassium phosphate at pH 6.7 for 12 h. The concentration of Mn-catalase was determined from the absorbance at 280 nm ($\epsilon_{280\text{ nm}} = 0.95\text{ mL mg}^{-1}\text{ cm}^{-1}$) and was in the range 20–25 mg/mL.

The chloride derivative of Mn-catalase, $\text{MnCat}(\text{II,II})(\text{Cl})$, in ammonium sulfate was obtained by a procedure similar to that described above. However, the enzyme was maintained as a crystalline precipitate form throughout the entire procedure. In this case 30 μL of the initial precipitate was loaded in an EPR tube covered by a dialysis membrane. The sample was then reduced by addition of 1 μL of 10 mM hydroxylamine sulfate. Excess hydroxylamine was removed by dialysis against 50% saturated ammonium sulfate. Subsequently, 5 μL of 700 mM potassium chloride was added to the sample prior to freezing in liquid nitrogen.

Liver Arginase. Purification of rat liver arginase is described in Reczkowski and Ash (1992). Samples contained 50 mM Hepes-KOH (pH 7.5) and either 0 or 10 mM borate and an enzyme concentration of 30–60 mg/mL.

EPR Spectroscopy. EPR spectra were obtained at 9.4 GHz on a Bruker ESP-300 spectrometer operating with a TE_{102} microwave rectangular cavity and Oxford Instrument ESR-900 and ESR-910 continuous-flow cryostats. Spectra were recorded using 100 kHz modulation frequency and modulation amplitude of 5 G.

An essential part of this study is EPR spectral deconvolution by multicomponent techniques, and intensity analysis over a wide temperature range of the signal areas. Quantitation of EPR signal areas at different temperatures requires the use of different microwave power levels in order to ensure both unsaturated conditions and optimal “signal to noise” ratio. For example, below 10 K the EPR signals of compound **1** used for evaluation of the temperature dependences presented in Figure 2 were detected at microwave powers less than 0.12 mW, whereas near 50 K the signal remains unsaturated even at 24.5 mW. A similar situation applied to all other samples except that the power levels chosen differed. In all cases unsaturated conditions were used. To compare unsaturated spectra detected at different microwave powers and temperatures, the signals were normalized by multiplying each of the experimental EPR spectra by the scaling factor of $T/(P)^{1/2}$, where T and P are the temperature and microwave power, respectively. This scaling factor normalizes signals which are not power saturated and removes the simple Curie temperature dependence.

RESULTS

Deconvolution of Experimental EPR Spectra. The line shapes and intensities of the EPR spectra of the $\text{Mn}_2(\text{II,II})$ proteins and compounds **1**, **2**, and **3** are a function of temperature in the interval 2.4–70 K. This dependence is illustrated in Figure 1 for $[\text{LMn}_2(\text{CH}_3\text{CO}_2)](\text{ClO}_4)_2$ dissolved in $\text{CH}_2\text{Cl}_2/n$ -butanol; spectra measured at 49.9 K and 17.1 K are shown in Figure 1, spectra a and c, respectively. The strong line shape dependence on temperature in this interval is not due to relaxation induced line broadening, as could be seen by the absence of any spectral broadening of the sharp ^{55}Mn hyperfine features which is evident in all of the samples (45 G splitting on each peak; see Figures 1, 3, and 5). The spectral changes observed as a function of temperature arise from the superposition of multiple spin states which could be separated by deconvolution into base spectra.

The deconvolution method we adopted assumed that the spectra are composed of a number of magnetic field dependent base spectra, labeled $e_i(H)$, whose line shape is independent of temperature, but whose intensity is governed by the Boltzmann equilibrium. This relationship is described by eq 1. In all samples studied here the EPR signals

$$e(H,T) = \frac{[n_1(T)e_1(H) + n_2(T)e_2(H)]}{T} \sqrt{P} \quad (1)$$

observed below 60 K and recorded under unsaturated conditions could be attributed to population of the two lowest excited electronic states (Boltzmann coefficients n_1 and n_2) above an EPR silent ground state of the $\text{Mn}_2(\text{II,II})$ species.

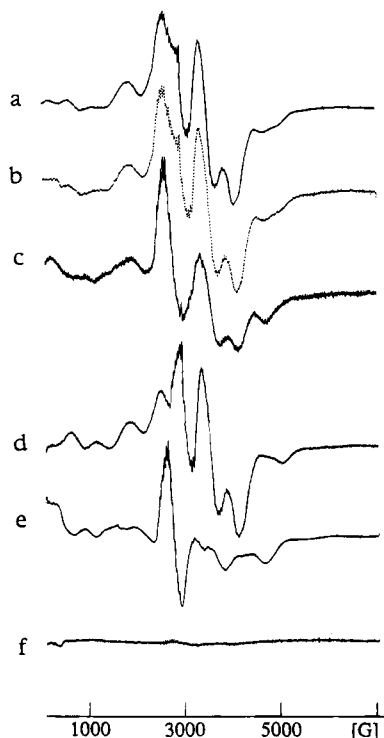


FIGURE 1: EPR signals of compound **1** recorded at (a) 49.9 K, 24.5 mW and (c) 17.1 K, 1.23 mW, respectively. (b) Reconstructed spectrum obtained as superposition of the base spectra e_2 (d) and e_1 (e), attributed to spin states $S = 2$ and $S = 1$, respectively (see eq 1). Populations n_1 and n_2 used in spectrum b are 0.470 and 0.189, respectively, at 49.9 K. (f) Residual spectrum obtained as the difference between experimental spectrum a and simulated spectrum b. For plotting purposes the original spectra a–f were multiplied by 1, 1, 5.2, 116, 0.75, and 1, respectively.

The quintet and triplet base spectra, e_2 and e_1 , of compound **1** are shown in Figure 1, spectra d and e, respectively. Figure 1b is the predicted superposition of these two base spectra at 49.9 K, obtained as the sum of e_2 and e_1 weighted by Boltzmann coefficients n_2 and n_1 , and thus should be compared to the spectrum in Figure 1a. The residual spectrum (Figure 1f) obtained as the difference between spectra a and b in Figure 1 demonstrates that the deconvolution into base signals e_1 and e_2 is quite satisfactory. The maximum deviation is less than 5%.

Below 10 K only the singlet ground state ($S = 0$) and first excited triplet state are significantly populated (compare spectra c and e). As the temperature is lowered below 4.2 K, the EPR signal disappears to give the baseline (not shown), and only the ground state is appreciably populated. Above 10 K a new spectrum grows in, resulting in the superposition of e_1 and e_2 (compare spectra d, e, and a). A similar temperature-dependent transformation of the EPR signals was observed for complexes **2** and **3** (Supplementary Material, Figures S1–S4).

The population coefficients, n_1 and n_2 , obtained from deconvolution of the EPR signals into base spectra are shown in Figure 2 as a function of temperature for compound **1**. These experimental coefficients are compared to the predicted Boltzmann populations of the two lowest excited electronic states arising from the Heisenberg exchange interaction, $-2JS(S + 1)$, between two Mn(II) ions. The Boltzmann coefficients describing the population of all six

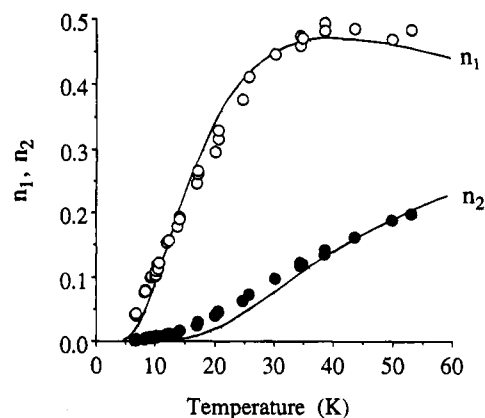


FIGURE 2: Experimental population coefficients n_1 and n_2 for the EPR signals of the triplet ($S = 1$) (○) and quintet ($S = 2$) (●) spin states, obtained by decomposition of EPR signal of compound **1** into base spectra e_1 and e_2 (Figure 1, spectra e and d), respectively. Solid lines are the predicted theoretical Boltzmann populations of the triplet (n_1) and quintet (n_2) states for a pair of spins, $S_1 = S_2 = 5/2$, coupled by an isotropic Heisenberg interaction $-2JS_1S_2$ with $J = -12 \text{ cm}^{-1}$.

possible spin states at thermal equilibrium are given by

$$n_s(T) = \frac{(2S + 1) \exp[-S(S + 1)J/T]}{\sum (2S_i + 1) \exp[-S_i(S_i + 1)J/T]} \quad S_i = 0, 1, \dots, 5 \quad (2)$$

Figure 2 reveals that there is good agreement between the experimental and theoretical populations for the two lowest excited spin states of $[\text{LMn}_2(\text{CH}_3\text{CO}_2)](\text{ClO}_4)_2$. Similar analyses have been done for compounds **2** and **3** which yield equally good agreement with the Boltzmann model (see Supplementary material, Figures S1–S4). The deduced Heisenberg exchange interaction constants (J) for complexes **1–3** are listed in Table 1. All three complexes are weakly antiferromagnetic with very similar J values of 12 cm^{-1} .

Assignment of the two base signals to a single $\text{Mn}_2(\text{II}, \text{II})$ chemical species was confirmed by additional tests performed with compound **1**. The relative concentrations of the two forms, n_1/n_2 , was found to be independent of the concentration of $\text{Mn}_2(\text{II}, \text{II})$ species, while the absolute intensities depend linearly on this concentration. Also, at any given temperature the same n_1/n_2 ratio was observed in several different preparations of the same material. Both results indicate a single chemical species is responsible for the two signals. In our initial studies of complex **3** (Mathur et al., 1987) the presence of a minor mononuclear Mn(II) impurity observable by its broad EPR signal at $g \approx 2$, lead to an incorrect determination of J . Because monomeric Mn(II) possesses a simple Curie temperature dependence, the signal from this species dominates spectra at low temperatures, even when present as a minor contaminant. This signal was used to monitor purification of the complexes during recrystallization to homogeneity and this impurity is absent in all samples studied here.

Zero-Field Splittings. A comparison of the ZFS in the EPR spectra of the triplet and quintet states of $[\text{LMn}_2(\text{CH}_3\text{CO}_2)](\text{ClO}_4)_2$ to those for $[\text{LMn}_2\text{Cl}_3]$ reveals that replacement of μ -acetate by μ -chloride changes both signals. For the triplet signal (Figure 1e) this replacement induces only a minor change in the position of the main peak (at 2700 G) and other peaks.

Table 1: X-ray Crystallographic and EPR ZFS Data for Mn(II)Mn(II) Centers

Mn(II) Mn(II) pair in	$r(\text{Mn-Mn}), (\text{\AA})$		$D_2 (\text{cm}^{-1})$	$D_1 (\text{cm}^{-1})$	$D_c (\text{cm}^{-1})$	$J (\text{cm}^{-1})$	reference ^s
	X-ray	ZFS					
MgO	3.06 ^a	3.07	-0.182	-0.776	0	-10.5	1-4
CaO	3.32	3.31	-0.126	-0.433	0	-2.8	1, 2
(CH ₃) ₄ NcCl ₃	3.26	3.25	-0.140	-0.666	+0.0041		5
[LMn ₂ (CH ₃ CO ₂)](ClO ₄) ₂ 1	3.54	3.57	-0.056	-0.28	(-)0.025 ^b	-12.0 ± 0.5	6-7, this work
LMn ₂ Cl ₃ 3		3.63	-0.041	-0.28	(-)0.025 ^b	-12.0 ± 0.5	6-7, this work
[(HL) ₂ Mn ₂ (μ-OH)](ClO ₄) 4	3.66 ^c	3.65	-0.034	-0.26		-2.65	8
MnCat ^d	3.6 ± 0.3						9
MnCat(Ph)		3.59	-0.051	-0.25		-5.6 ± 0.1	this work
arginase(+borate)		3.50	-0.073			-2.0 ± 0.5	this work
arginase(-borate)		3.57	-0.056				
		3.52	-0.069				
		3.36	-0.105				
alkaline phosphatase	4			nd ^e	0.083 ^e		10
concanavalin A	4.25			-0.038 ^f	(-)0.023 ^f		11, 12

^a Underlined numbers were used for D_2 calibration presented in Figure 8. ^b The absolute D_c value was determined based on analysis of EPR spectra of the mixed metal species [LMnZn(CH₃CO₂)₂]²⁺ (Khangulov, Pessiki, et al., unpublished results). Negative D_c but not positive value fits eq 4. ^c Mn-Mn distance derived from X-ray analysis of Zn-substituted **4** (Flassbeck et al., 1992). An H_{hf} value of 4420 G was used to calculate D_2 (see text). ^d Mn-Mn distance obtained from X-ray analysis for single crystal soaked in ammonium sulfate. ^e No evidence for exchange interaction between Mn(II) ions in the A and B sites at 4 Å apart; Mn ions do not share a bridging ligand. ^f For the dimanganese(II,II) protein. ^s (1) Owen and Harris (1972). (2) Harris (1972). (3) Coles et al. (1960). (4) Harris and Owen (1963). (5) Heming et al. (1982). (6) Pessiki et al. (1994a). (7) Pessiki et al. (1994b). (8) Flassbeck et al. (1992). (9) Barynin et al. (1986) and Barynin (1991). (10) Schultz et al. (1989). (11) Antanaitis et al. (1987). (12) Meirovitch et al. (1974).

The line shape of the quintet signal (Figure 1d) is slightly transformed upon replacement of μ -acetate in **1** by μ -Cl⁻ in **3**. One pronounced difference is a shift of the highest field peak (marked in Figure 7 by arrow) from 5100 G (Figure 1d) to 4640 G (Supplementary material, Figure S1c). According to the analysis given in the Discussion, this shift corresponds to a 25% smaller range of ZFS observed for the μ -Cl⁻ derivative **3** in the quintet state.

MnCat(II,II)(phosphate). The phosphate derivative of Mn-catalase in the Mn₂(II,II) oxidation state, MnCat(II,II)(Ph), exhibits a strong non-Curie temperature dependence originally attributed to population of a single excited triplet state. This earlier conclusion was made on the basis of the temperature dependence of one of the hyperfine lines of the signal (Khangulov et al., 1986, 1990b). Using the multi-component analysis method, here we find that below 70 K the observed spectrum is the sum of three base spectra, e_1 , e'_2 , and e''_2 (Figure 3A), attributed to the first and second excited spin states which lie above an EPR silent ground state.

The raw spectra at 47.1 and 9.0 K are given in Figure 3B, spectra a and c, respectively. It was found that spectra obtained below $T \sim 30$ K could be well represented as the sum of the two base signals, e_1 and e'_2 , while the signal detected above $T \sim 30$ K requires an additional base signal e''_2 to be included for accurate fits, corresponding to adding a third term to eq 1, $[n''_2(T)e''_2(H)]/T$. At 47.1 K the e''_2 signal is about one-third the amplitude of the e'_2 signal. The e''_2 signal has the same line shape as the e'_2 signal (compare Figure 3A spectra a and b) but is broader and lacks all resolved hyperfine features. Accordingly, we assign this also to a quintet spin state like the e'_2 species, but from a different population of enzyme having a faster relaxation time. Because these signals are considered to have the same spin, the same intrinsic EPR transition probabilities were assumed in obtaining the Boltzmann population coefficients in Figure 4.

A plot of the temperature dependence of the population coefficients, n_1 , n'_2 , and n''_2 , is shown in Figure 4 and

compared to the Boltzmann populations predicted for the triplet and quintet excited states using the Heisenberg expression, eq 2. The population n_1 of e_1 agrees well with the predicted intensity dependence of the triplet state, while the sum $n'_2 + n''_2$ agrees reasonably well with the predicted quintet state population. This analysis yields a revised exchange constant of $J = -5.6 \text{ cm}^{-1}$, compared to -14.4 cm^{-1} for an earlier result in which only a single excited (triplet) state for the EPR signal was proposed (Khangulov et al., 1986, 1990b).

The spectrum reconstructed from the base spectra at 47.1 K is presented in Figure 3B, spectrum b, and uses the Boltzmann populations n_1 , n'_2 , and n''_2 of 0.323, 0.190, and 0.070, respectively. This reconstructed spectrum is seen to accurately represent the experimental spectrum given in Figure 3B, spectrum a, as seen by the negligible residual spectrum (Figure 3B, spectrum d) obtained as the difference between spectra a and b.

MnCat(II,II)(Cl). Formation of the chloride adduct of MnCat(II,II) was verified by comparison to the previously reported EPR spectrum (Khangulov et al., 1987). As previously noted, the spectrum reveals a multiline ⁵⁵Mn hyperfine pattern with 45–46 G splitting and a non-Curie temperature dependence, both of which are consistent with a spin-coupled Mn₂(II,II) formulation (Figure S5). Analysis of the temperature dependence of the whole EPR spectrum indicates, however, that the signal is a complex superposition of several EPR signals. For this reason we were unable to make an accurate deconvolution of the spectrum and hence could not clearly identify base spectra for the excited spin states nor estimate the exchange integral. This problem presumably stems from either incomplete binding of Cl⁻ or multiple Cl⁻ binding sites which would require a detailed titration study that we did not pursue.

Arginase(II,II). Although it has been known for some time that liver arginase is a Mn-dependent enzyme, it was only recently shown to possess a spin-coupled Mn₂(II,II) active site, based on the ⁵⁵Mn hyperfine structure (Reczkowski & Ash, 1992). Analysis of the temperature dependence of the

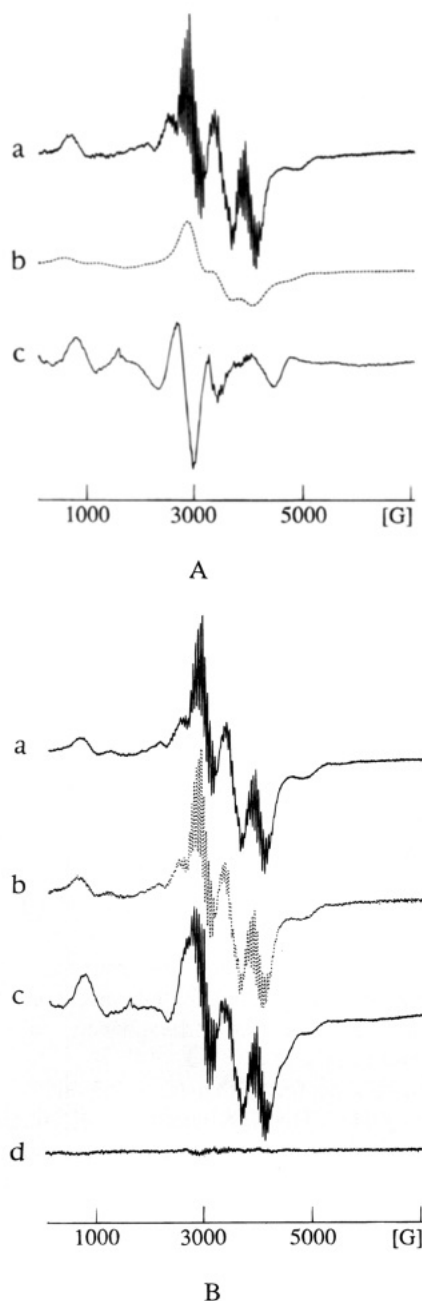


FIGURE 3: (A) EPR base spectra e'_2 (a), e''_2 (b), and e_1 (c) obtained by spectral deconvolution of the EPR signals of the phosphate complex of Mn-catalase(II,II) between 4 and 60 K. Spectra a and c are attributed by the quintet and triplet states, respectively. Spectrum b appears only above $T > 30$ K and is attributed to the same quintet state, but with a broader line shape due to spin-lattice relaxation. (B) EPR signal of MnCat(II,II)(Ph) recorded at (a) 47.1 K, 15.8 mW and (c) 9.0 K, 3.2 mW, respectively. (b) Reconstructed spectrum at 47.1 K obtained as the sum of base spectra e_1 , e'_2 , and e''_2 , presented in panel A, weighted by the Boltzmann coefficients n_1 , n'_2 , and n''_2 of 0.323, 0.190, and 0.070, respectively. (d) Residual spectrum obtained as the difference between the experimental (a) and simulated (b) spectra. For display purposes the original spectra a–c in panel A and spectra a–d in panel B were multiplied by 55, 27.5, 1.55, 0.9, 0.9, 2.63, and 0.9, respectively.

EPR signal intensity reveals a non-Curie behavior and diamagnetic ground state similar to, but with much smaller energy gap than, that observed for complexes **1–3** and MnCat(Ph). EPR spectra of borate-free and borate-containing enzyme are presented in Figure 5A, spectra a and b, respectively. These spectra reveal that there are changes in the ZFS upon addition of the inhibitor borate. As noted in

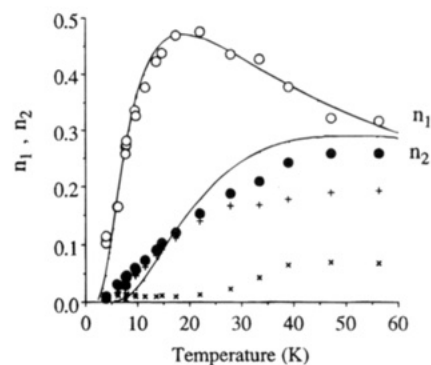


FIGURE 4: Temperature dependence of the population coefficients n_1 (○), n'_2 (+), n''_2 (×), and $n_2 = n'_2 + n''_2$ (●) obtained by decomposition of the EPR signal of MnCat(II,II)(Ph) into the basis spectra e_1 , e'_2 , and e''_2 . Solid lines are the predicted Boltzmann populations for the triplet and quintet spin states with $J = -5.6$ cm^{-1} .

Figure 5C, an expansion of the ZFS observed on the high field side of the spectrum becomes simpler upon the addition of borate, collapsing from three resolved peaks (–borate) to a single broad shoulder with resolved ^{55}Mn hyperfine structure (+borate).

Figure 6 presents the temperature dependence of the EPR spectrum of the borate containing enzyme and compares it to the predicted Boltzmann population for an excited quintet state using the Heisenberg model with $J = -2.0 \pm 0.5$ cm^{-1} . The agreement is reasonable, and there seems to be little need on the basis of these data to include more than a single excited spin state.

We assign the arginase spectrum in Figure 5 to predominantly the quintet state on the basis of an additional observation. There is a pronounced similarity between the arginase spectrum and the quintet signal from compounds **1**, **2**, and **3**; the triplet spectra of the latter species have very different line shapes than their corresponding quintet spectra. The predicted J value for arginase is a factor of 6 smaller than that observed for complexes **1–3** and 2–3 times smaller than for the phosphate derivative of MnCat, as summarized in Table 1. This small J value means that for arginase the strongest temperature dependence of the EPR signal should occur at much lower temperatures than for compounds **1–3**, where population of the triplet state should dominate. We measured the temperature dependence of the arginase EPR signal using a He immersion cryostat in the range 1.9–3.6 K (Oxford ESR-910). However, we were unable to observe sufficiently intense spectra needed for reliable deconvolution by multicomponent analysis, owing to the need to use exceedingly low microwave powers to avoid saturation of the signal. Thus for arginase the deconvolution method is much less effective over the temperature and microwave powers ranges where we could obtain good data.

DISCUSSION

The methods reported here can be used to evaluate two parameters which are strongly dependent on the Mn–Mn distance and chemical bonding; the Heisenberg exchange integral and the ZFS in the excited $S = 2$ state (D_2). The next section discusses the ZFS, while the last section discusses the Heisenberg interaction.

Determination of Mn–Mn Distance from Zero-Field Splitting of EPR Spectra. The theory developed by Owen and Harris (1972) establishes the connection between the

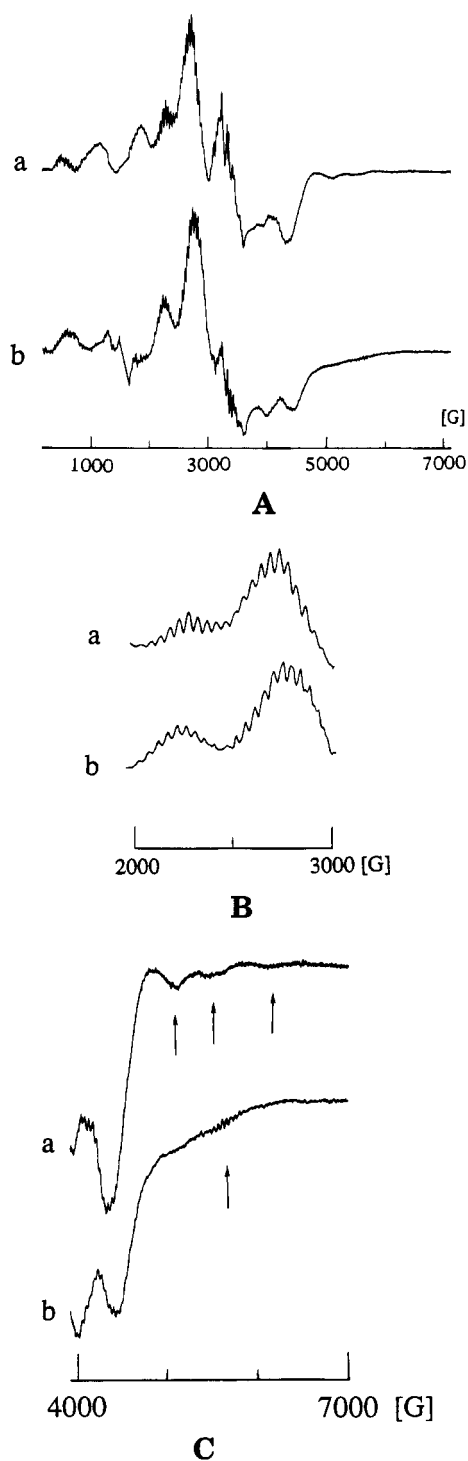


FIGURE 5: (A) EPR spectra of liver arginase (a) and the complex of arginase with borate (b) detected at 20 K and 12.8 mW. Panels B and C illustrate ^{55}Mn hyperfine structure and ZFS in the 2200–3200 and 4000–7000 G regions of the spectra presented in panel A. Arrows indicate the position of the high field (H_{hf}) EPR transitions used for estimation of D_2 values (see text).

Mn–Mn distance (r) and the ZFS parameters of the complex, D_c and D_s . D_c and D_s are the single ion ZFS of the individual Mn(II) ions and the dimer ZFS in spin states S , respectively.

In the case of axial symmetry, the effective spin hamiltonian applicable to each spin state of a dimer is given by

$$H = g\beta HS + D_s[S_z^2 - (1/3)S(S+1)] \quad (3)$$

D_s may be expressed using two terms; the magnetic dipole–

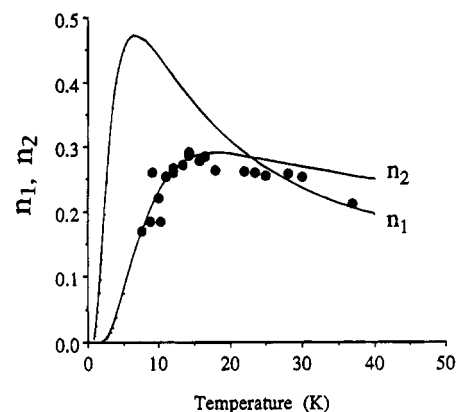


FIGURE 6: Temperature dependences of the EPR signal of liver arginase(II,II)(borate) (●). Solid lines are the predicted Boltzmann populations of the triplet and quintet spin states calculated for $J = -2.0 \text{ cm}^{-1}$.

dipole interaction, $-(g\beta)^2/r^3$, and the single ion crystal field splitting, D_c , using eq 4. The dipolar interaction tensor

$$D_s = \beta_s D_c - [3\alpha_s(g\beta)^2/r^3] \quad (4)$$

between two Mn(II) ions is accurately modeled as an axial tensor for the present studies where there is little transfer of spin onto the ligands and the Mn ions are much further apart than the diameter of each ion. The coefficients, α_s and β_s , are derived from vector coupling formulae as a function of the electronic spin (S). For the $S = 1$ and 2 states derived from two $S_i = 5/2$ Mn(II) ions, these are $\alpha_1 = +37/10$, $\beta_1 = -32/5$, $\alpha_2 = +41/42$, and $\beta_2 = -20/21$. Consequently, measurement of the experimental D_s from the EPR signal, along with a knowledge of the spin state origin and the single ion ZFS enables determination of the magnetic dipole–dipole interaction and finally r .

For all samples we found that $D_2 < 0.3 \text{ cm}^{-1} = \text{Zeeman energy at } 9.4 \text{ GHz}$. The ZFS is not linearly related to the spectral splitting but must be obtained by spectral simulation or by fitting to the expression for transition frequencies. We adopted the latter procedure, using the convenient spectral diagrams derived for the case of axial ZFS (Baranowski et al., 1979; DeVore et al., 1978; Van Zee et al., 1979; Dowsing, 1970; Dowsing & Gibson, 1969; Van Zee & Weltner, 1981). These diagrams give the positions of the EPR transitions for a system of randomly oriented particles of known spin.

Our approach is illustrated in Figure 7 which compares the EPR spectrum of compound 1 to the predicted transitions at the parallel (solid lines) and perpendicular turning points (dashed lines) for a randomly oriented quintet spin state as a function of $D_2/h\nu$ (Baranowski et al., 1979). The horizontal dashed line is drawn at $D_2 = 0.056 \text{ cm}^{-1}$ where it intersects the resonance magnetic field positions in close correspondence with the turning points observed in the experimental spectrum (Figure 7, bottom). This value of D_2 predicts correctly the positions of all six of the high field transitions above 1000 G. Two weaker transitions occur below 1000 G, but the theory becomes less reliable at these low field strengths and so were not considered in the analysis. In order to determine the D_2 value, we used the highest field peak, H_{hf} , of the experimental spectrum of the quintet state, which is marked by the arrow in Figure 7 (bottom). This peak is the most accurately predicted by the theory and also does

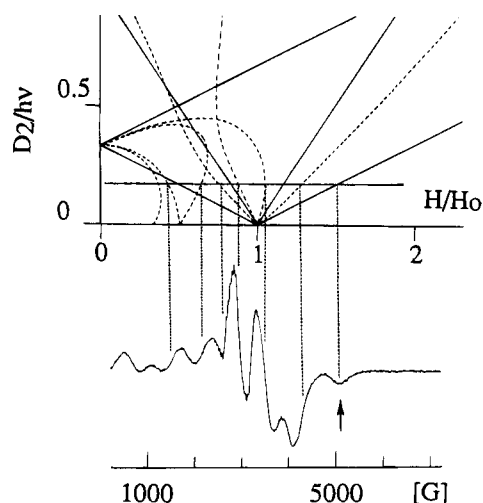


FIGURE 7: Application of the theoretical diagram developed by Baranowski et al. (1979) for determination of the ZFS for quintet spin states with axial symmetry. (Top) Resonance field dependence on the magnitude of the ZFS parameter D_2 for $H \parallel z$ (solid lines) and $H \perp z$ (dotted lines), $g = 2.0023$. The horizontal dotted line corresponds to a D_2 value of 0.056 cm^{-1} . (Bottom) EPR signal for the quintet state of compound 1.

not interfere with other transitions in the experimental spectra. In this case, the D_2 value can be estimated from the expression $|D_2|/h\nu = 0.34(H_{\text{hf}}/H_0 - 1)$, which is an analytical expression for the magnetic field dependence of the highest transition presented in Figure 7 (top).

The H_{hf} values for complexes 1, 3, MnCat(II,II)(Ph), and Arg(II,II)(borate) are 5100, 4640, 4940, and 5650 G, respectively. In the absence of borate, the high field component of the arginase EPR signal reveals three maxima at 5100, 5500, and 6650 G (Figure 5C, spectrum a). The corresponding D_2 values are given in Table 1. In this case, addition of the active site inhibitor borate simplifies the ZFS by converting the three peaks to a single broad shoulder (Figure 5C, spectrum b). This result suggests that two or three conformational states exist in aqua Arg(II,II), having Mn–Mn distances in the range 3.36–3.57 Å, which can be converted to fewer conformational species by addition of borate, possibly as few as one species at 3.50 Å. The addition of borate eliminates the peak at 6650 G corresponding to the shortest Mn–Mn separation of 3.36 Å, while replacing the remaining two peaks by a single peak with well resolved dimeric ^{55}Mn hyperfine structure. The appearance of resolved hyperfine structure indicates a narrower distribution of conformational states which are populated. This may reflect either direct coordination of borate, or possibly interaction of borate with ligands to Mn, as depicted in Figure 9B.

Analysis of the EPR spectra does not give the sign of the ZFS. We found, however, that the dimer $|D_2|$ values are much larger than the monomer $|D_c|$ values for all $\text{Mn}_2(\text{II,II})$ compounds for which both sets are available (see Table 1). This observation enables us to conclude that the negative sign of the magnetic dipole–dipole interaction in eq 4 predominates so that the sign of D_2 must be negative.

Extraction of metrical information from D_2 by direct application of the theory and particularly eq 4 is limited because the single ion ZFS value (D_c) and the relative orientation of the D_c tensor to the magnetic dipole–dipole interaction tensor are not known for all of the complexes

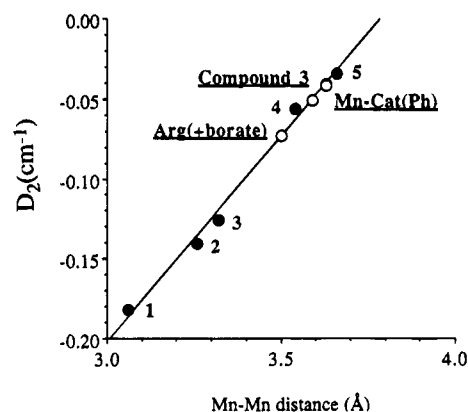


FIGURE 8: Correlation (solid line) between the crystallographically determined Mn–Mn distance and the EPR determined ZFS of the quintet state (D_2) for five examples (underlined) for which both data sets are available (Table 1). Points 1, 2, and 3 are for $\text{Mn}_2(\text{II,II})$ pairs in crystal lattices of MgO , $(\text{CH}_3)_4\text{NCdCl}_3$, and CaO , respectively. Points 4 and 5 correspond to compounds 1 and 4, respectively. Open circles (○) indicate Arg(+borate), MnCat(Ph), and compound 3.

studied here (Smith & Pilbrow, 1974). However, there is a good linear correlation between the crystallographically determined Mn–Mn distance and the EPR determined D_2 value for five examples for which both data sets are available, as graphed in Figure 8 and summarized in Table 1. Also included in this correlation is a μ -hydroxo bridged $\text{Mn}_2(\text{II,II})$ compound 4 reported by Flassbeck et al. (1992). Application of the empirical correlation in Figure 8 to the Mn–Mn separation in $[\text{LMn}_2\text{Cl}_3]$ gives 3.63 Å. This value should be accurate to ± 0.03 Å using the maximum deviation for the five standards in Figure 8. The correlation presented in Figure 8 predicts a Mn–Mn distance of 3.59 Å for MnCat(Ph). These results are consistent with the Mn–Mn distance of 3.6 ± 0.3 Å obtained previously by X-ray crystallography of Mn–catalase crystals obtained from ammonium sulfate (Barynin et al., 1986, 1991).

The empirically observed linear correlation between D_2 and the Mn–Mn separation implies, according to eq 4, that $|D_c|$ must decrease at shorter Mn–Mn separations since the dipole–dipole component of D_2 increases as r^3 . In other words, the axial ligand field potential which determines $|D_c|$ becomes more symmetric (decrease in $|D_c|$) upon approach of the second metal ion. That such a correlation exists should not be surprising considering that the ligand field strength of the bridging ligand should decrease as the second metal ion approaches. If the second metal could be removed, we would expect that the bridging ligand (O^{2-} , OH^- , RO^-) would present a stronger electrostatic potential than any of the remaining ligands and therefore be the major determinant of $|D_c|$.

A decrease in $|D_c|$ caused by the presence of a μ -ligand is also evident in the $\text{Mn}_2(\text{II,II})$ site of alkaline phosphatase (Schultz, 1989). This enzyme has two Mn(II) ions, denoted sites A and B, which are separated by approximately 4 Å. The exchange interaction between MnA and MnB is too small to be detected at both Q- and X-band EPR frequencies, and the lack of interaction was attributed to the fact that the Mn ions do not share a bridging ligand. The Mn(II) ions exhibit an unusually high $|D_c|$ value of 0.083 cm^{-1} , which is 2–4 times larger than observed for Mn(II) ions which share a bridging ligand and are coupled by an exchange interaction (see Table 1). In another example, the carbohy-

drate binding protein concanavalin A, which has Ca^{2+} and Mn^{2+} ions separated by 4.25 Å has been found to exhibit a small $|D_c|$ value of 0.023 cm^{-1} (Meirovitch et al., 1974). The presence in ConA of two μ -carboxyl bridges (Asp10 and Asp19) has been established by X-ray diffraction (Hardman et al., 1982) and is presumed to provide the dominant pathway responsible for the weak antiferromagnetic coupling between the Mn^{2+} ions in the dimanganese derivative of this protein (J is about -0.9 cm^{-1} ; Antanaitis et al., 1987). This example agrees with the correlation between small $|D_c|$, i.e., higher symmetry of the ligand field around Mn(II) , and the presence of a second divalent metal coordinated by one or more bridging ligands. Thus, a possible role for the second metal ion in μ -bridged dimetalloproteins may be to lower the μ -ligand field potential, thereby increasing the oxidation potential of both metals and increasing the ligand field strength of the remaining (terminal) ligands. The former outcome would be relevant to the functioning of redox proteins, while the latter outcome might provide a means for activation of substrate bound to only one metal ion. A weakened μ -ligand field potential may play a role, for example, in promoting ionization of a proton from a manganese bound water molecule in arginase, with the resulting hydroxide ligand being the nucleophile needed for hydrolysis of substrate.

Conclusions from Heisenberg Exchange and ZFS. The accuracy of the spectral deconvolution method determines the accuracy for estimation of the temperature coefficients given in Figures 2 and 4 and thus sets the limits for estimation of J . The spectral deconvolution results indicate that good agreement between the experimental spectra and the reconstructed spectra can be obtained below 60 K using the Heisenberg exchange ladder for energies and the Boltzmann model for populations (Figure 1, spectrum f, and Figure 3B, spectrum d).

The Heisenberg exchange interaction constants for compounds **1**, **2**, and **3** are nearly identical (about -12.0 cm^{-1}) (Table 1). Thus, replacement of the μ -acetato by μ -Cl does not change noticeably the strength of the antiferromagnetic interaction. An extensive summary of the literature data on the Heisenberg exchange constant of several $\text{Mn}_2(\text{II,II})$ complexes is presented in Table 2. These values were obtained primarily by variable temperature magnetic susceptibility measurements. Our assignment of the two excited state EPR signals in complexes **1–3** and $\text{MnCat}(\text{II,II})$ to triplet and quintet spin states is consistent with the conclusions reached by Flassbeck et al. (1992), who studied μ -hydroxo-bridged $\text{Mn}_2(\text{II,II})$ complexes derived from the pentadentate macrocyclic ligand 4,7-bis(2-hydroxybenzyl)-1-oxa-4,7-diazacyclononane $[(\text{L}_1\text{H})_2\text{Mn}_2(\text{m-OH})](\text{ClO}_4)$ (compound **4**, Table 2). On the basis of comparisons of the temperature dependence of magnetic susceptibility to the EPR signal, compound **4** was found to populate triplet and quintet states.

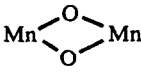
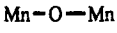
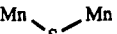
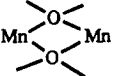
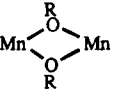
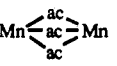
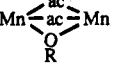
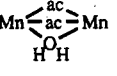
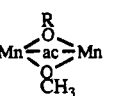
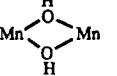
Generally, simple arguments based on orbital overlap and orbital energies are often sufficient to explain the magnetic properties of Mn(II) clusters, owing to the spherically symmetrical unpaired spin distribution achieved by the $3d^5$ electronic configuration. As expected, the J value depends on the type of bridging groups which span the Mn(II) ions, the Mn–Mn distance, and the Mn–X–Mn angle. The decrease of J with increasing Mn–Mn distance is illustrated for the $\text{Mn}(\mu\text{-O})_2\text{Mn}$ unit formed in edge shared sites in MgO

($r = 3.06 \text{ Å}$), MnO ($r = 3.13 \text{ Å}$), and CaO ($r = 3.32 \text{ Å}$) where J (cm^{-1}) decreases in the series from -10.5 , -6.9 to -2.8 . A stronger antiferromagnetic coupling pathway is produced in the linear $[\text{-Mn}(\mu\text{-O})\text{Mn-}]^{2+}$ unit formed between Mn(II) ions occupying sites which share only a single corner oxide anion in MgO ($r = 4.30 \text{ Å}$, $J = -19.6 \text{ cm}^{-1}$) and CaO ($r = 4.45 \text{ Å}$, $J = -3 \text{ cm}^{-1}$). This comparison indicates that, with proper choice of distance, either di- μ -oxo or mono- μ -oxo bridges could produce antiferromagnetic coupling interactions comparable to the range of values which we observe for complexes **1–3**, $\text{MnCat}(\text{II,II})(\text{Ph})$, and $\text{Arg}(\text{II,II})$.

The μ -alkoxide bridge is common to complexes **1–3** which exhibit equivalent J values (Table 1). These J values are somewhat larger (28–33%) than for complexes possessing the $(\mu\text{-OH})(\mu\text{-carboxylato})_2$ bridging unit (-9 cm^{-1}), even though the Mn–Mn separation is shorter by 0.2 Å (Table 2). Presumably this behavior reflects the stronger antiferromagnetic coupling mediated by the alkoxide bridge of **L** which occurs upon opening the angle to a more linear geometry (119.4° in **1**; Pessiki et al., 1994a), as was noted above for the bent and linear sites in MgO and CaO . On the other hand, both bis(μ -phenoxide) and bis(μ -carboxylato)-(μ -aqua) bridging groups produce much weaker couplings than we observe for all $\text{Mn}_2(\text{II,II})$ species except $\text{Arg}(\text{II,II})$. This is expected on the basis of the nearly orthogonal angular geometry within the $\text{Mn}_2(\mu\text{-OPh})_2$ rhombus ($94\text{--}104^\circ$) and the poor superexchange pathway via the aqua ligand, respectively. Table 1 indicates that the exchange coupling observed for $\text{MnCat}(\text{II,II})(\text{phosphate})$ species (-5.6 cm^{-1}) is intermediate between that for $[\text{L}_2\text{Mn}_2(\mu\text{-OAc})_2(\mu\text{-OH})]^+$ (-9 cm^{-1}) and $[\text{L}_2\text{Mn}_2(\mu\text{-OAc})_2(\mu\text{-H}_2\text{O})]^{2+}$ (-1.65 to -2.95 cm^{-1}). Moreover, the Mn–Mn distance of $3.59 \pm 0.03 \text{ Å}$, obtained for the enzyme from the ZFS calibration (Figure 8), is also intermediate between these structural units. One possible way to achieve both of these features would be if the reduced enzyme also possesses the $[\text{Mn}_2(\mu\text{-carboxylato})_2(\mu\text{-H}_2\text{O})]^{2+}$ unit, but having additional internal hydrogen-bonding of the μ -aqua protons to protein or solvent acceptor ligands so that the superexchange pathway approaches the $\mu\text{-OH}^-$ limit as depicted in Figure 9A. Analogously, a protein or solvent derived hydrogen-bond donor to a $\mu\text{-OH}^-$ bridge in $[\text{Mn}_2(\mu\text{-carboxylato})_2(\mu\text{-OH})]^+$ would produce the same result. Other structural proposals are possible. This proposed bridging structure agrees well with that proposed for the oxidized enzyme, $[\text{MnCat}(\text{III,III})(\mu\text{-carboxylato})_{1-2}(\mu\text{-O})]^{n+}$, on the basis of electronic absorption data (Sheats et al., 1987), and with the superoxidized state, $[\text{MnCat}(\text{III,IV})(\mu\text{-carboxylato})_{0-1}(\mu\text{-O})_2]^{n+}$, on the basis of EPR, ENDOR, and Mn-EXAFS data (Waldo et al., 1992; Zheng et al., 1993). Thus, we propose protonation of the oxo bridge upon reduction to $\text{MnCat}(\text{II,II})$, yielding $(\mu\text{-carboxylato})_{1-2}(\mu\text{-OH})$ or $(\mu\text{-carboxylato})_{1-2}(\mu\text{-OH}_2)$.

Transformation of the EPR line shape of $\text{MnCat}(\text{II,II})$ upon replacing the bound inorganic phosphate by Cl^- , as well as many other anions including F^- , N_3^- , acetate, etc. (Khangulov et al., 1987), and the fact that both chloride and phosphate are potent inhibitors of catalase activity suggests that anions may bind directly to the $\text{Mn}_2(\text{II,II})$ site and thereby block the cycle of hydrogen peroxide decomposition (Khangulov et al., 1990b,d,e). However, it remains unclear if anions bind to a bridging or terminal site on Mn, as depicted in Figure 9A. Although a direct effect via a bridging site would seem

Table 2: Exchange Integrals J for Different $Mn_2(II,II)$ Dimers ($H = -2JS_1S_2$)^a

	compound ^b	J /(cm)	r (Å)	M—O—M (deg)	reference
	in MgO	−10.5	3.06		
	in MnO	−6.9	3.13		
	in CaO	−2.8	3.32		Harris (1972) and Owen and Harris (1972)
	in MgO	−19.6	4.3	180	
	in CaO	−3	4.45		
	μ -thiolate [Mn(¹ L)Cl(CH ₃ OH)] _n	−7.8	4.67	127.7	Mikuriya et al. (1991)
	bis(μ_4 -O ^{2−}) Mn ₆ O ₂ (O ₂ CPh) ₁₀ (py) ₂ (MeCN) ₂	−2.4	3.8	117.4, 119.9	Schake et al. (1989)
	bis(μ -phenoxo) [Mn ₂ (² L) ₂ (THF) ₂](ClO ₄) ₂	> −0.18	3.256	99.9	Hodgson et al. (1989)
	[Mn ₂ (³ L) ₂ (NCS) ₂]		3.422	104.1	Nishida (1987)
	[Mn(⁴ L)] ₂	−0.63			Mabad et al. (1986)
	[Mn(⁵ L)] ₂	−1.88	3.3	101.2	Kessissoglou et al. (1987)
	[Mn(⁶ L)CH ₃ CN] ₂		3.205	93.6	Yu et al. (1991, 1992)
	[Mn ₂ (⁷ L) ₂ Cl ₂]	+0.24	3.324	103.2	Chang et al. (1988)
	[Mn ₂ (⁸ L)Cl ₂]	+0.2			Lamabert et al. (1979)
	[Mn ₂ (⁹ L)(CH ₃ CO ₂) ₂]		3.34	103.6	Downard et al. (1990)
	tris(μ -carboxylato) [Mn ₂ (¹⁰ L)(μ -CH ₃ CO ₂) ₃] ⁺	−1.7	4.034		Wieghardt et al. (1988)
	bis(μ -carboxylato) dimanganese concavalin A [Mn ₂ (C ₃ F ₇ CO ₂) ₄ (bipy) ₂]	−1.8 −2.6	4.25 3.679		Antanaitis et al. (1987) Menage (1988)
	(μ -phenoxo)bis(μ -carboxylato) [Mn ₂ (¹¹ L)(CH ₃ CO ₂) ₂] ⁺	−4.9			Suzuki et al. (1987)
	[Mn ₂ (¹¹ L)(PhCO ₂) ₂] ⁺	−5.5			Suzuki et al. (1987)
	[Mn ₂ (¹² L)(CH ₃ CO ₂) ₂] ⁺		3.589	115.8	Gulntneh et al. (1992)
	[Mn ₂ (¹³ L)(NCS)(CH ₃ CO ₂) ₂]		3.34	99.9	Mikuriya et al. (1990)
	(μ -H ₂ O)bis(μ -carboxylato) [Mn ₂ (¹⁴ L)(F ₃ C ₂ CO ₂) ₄ (H ₂ O) ₃]	−1.65	3.739	114.6	Caneschi et al. (1989)
	[Mn ₂ (H ₂ O)(piv) ₄ (Me ₂ bpy) ₂]	−2.73	3.595	110.2	Yu et al. (1992)
	[Mn ₂ (H ₂ O)(CH ₃ CO ₂) ₄ (¹⁵ L) ₂]	−2.952	3.621	110.0	Yu et al. (1992)
	[Mn ₂ (¹⁶ L)(NCS)(CH ₃ CO ₂) ₂]	−3.5 ± 1.5	3.325	99.2	Sakiyama et al. (1993)
	(μ -hydroxo)bis(μ -carboxylato) [Mn ₂ (¹⁰ L)(μ -OH)(μ -CH ₃ CO ₂) ₂] ⁺	−9	3.351	109.4	Bossek et al. (1989)
	(μ -alkoxo)(μ -carboxylato) (μ -phenoxo) Mn ₂ (¹³ L)(CH ₃ O)(CH ₃ CO ₂) ⁺	−3.8			Mikuriya et al. (1989)
	μ -hydroxo [Mn ₂ (¹⁷ L) ₂ (μ -OH)] ⁺	−2.65			Flassbeck et al. (1992)
	bis(μ -hydroxo) [Mn ₂ (¹⁸ L) ₂ (OH)] ₂		3.314	104.8	Kitajima et al. (1991)

^a For Mn complexes in Mn₂(II,III) and Mn₂(III,IV) redox state, see Que and True (1990). ^b Ligands (ⁱL, $i = 1, 2, 3, \dots$): 1 = 2-[2-(2-pyridyl)ethylamino]ethanethiol = ¹L; 2 = *o*-(bis(2-(1-pyrazolyl)ethyl)amino)phenol; 3 = 2-[bis(2-pyridylmethyl)aminomethyl-4-nitrophenol]; 4 = *N,N'*-bis(salicylidene)-1,7-diamino-3-azapentane; 5 = *N,N'*-[1,1'-dithiobis(phenylene)]bis(salicylideneamino)methylphenol; 6 = 2-(bis(salicylideneamino)methylphenol); 7 = Schiff base of 1,3-diaminopropane and 2 mol of 2,6-diformyl-4-methylphenol; 8 = Schiff base of 1,3-diaminopropane and 2 mol of 2,6-diformyl-4-methylphenol; 9 = Schiff base of 1,3-diamino-2-hydroxypropane and 2 mol of 2,6-diformyl-4-methylphenol; 10 = *N,N',N''*-trimethyl-1,4,7-triazacyclononane; 11 = 2,6-bis[bis(2-pyridylmethyl)aminomethyl]-4-methylphenol; 12 = 2,6-bis[bis(2-(2-pyridyl)ethyl)amino]methylphenol; 13 = 2,6-bis[*N*-(2-pyridylethyl)iminomethyl]-4-methylphenol; 14 = 2-ethyl-4,4,5,5-tetramethyl-3-oxo-4,5-dihydro-1*H*-imidazolyl-1-oxyl; 15 = *N,N,N',N'*-tetramethylethylenediamine; 16 = 2,6-bis[2-(diethylamino)ethylaminomethyl]-4-methylphenolate; 17 = 4,7-bis(2-hydroxybenzyl)-1-oxa-4,7-diazacyclononane; 18 = hydrotris(3,5-diisopropyl-1-pyrazolyl)borate.

to offer the simplest explanation for the EPR ZFS change via the dipolar term, it is also possible that binding to a terminal site could impart a structural change sufficient to alter the ZFS.

The considerably weaker exchange interaction observed for Arg(II,II)(borate) indicates either a greater Mn—Mn distance or further weakening of the superexchange pathway

than is present in complexes 1–3 or MnCat(II,II)(Ph). Since the Mn—Mn distance, determined from analysis of the ZFS, is slightly shorter in the borate derivative of Arginase than in complexes 1–3, we are lead to the latter explanation. As described above, one possible means for weakening of ligand-mediated superexchange is by successive protonation of μ -O to μ -OH and to μ -OH₂. Arg(II,II) falls in the class

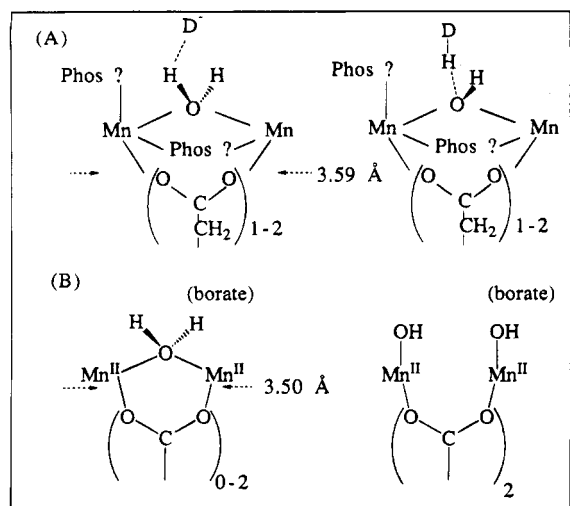


FIGURE 9: (A) Possible EPR deduced structures of MnCat(II,II)-(Ph) suggesting hydrogen-bonded μ -aqua/ μ -hydroxo bridge on the basis of Heisenberg exchange, μ - or terminal phosphate on the basis of ZFS, and carboxyl(s) on the basis of extrapolation from MnCat-(III,III) and MnCat(III,IV); see text. D^- is a proton acceptor. (B) Possible EPR deduced structures of arginase(II,II)(borate) on the basis of Heisenberg exchange and ZFS.

of weak superexchange interactions and Mn-Mn separations which are compatible with the $(\mu\text{-OH}_2)(\mu\text{-carboxylato})_{1-2}$ or $(\mu\text{-OH})(\mu\text{-carboxylato})_{0-2}$ bridging unit, as depicted in Figure 9B. Alternatively, the 2–3-fold weaker exchange interaction in Arginase(II,II)(borate) vs MnCat(II,II)(Ph) may reflect an appreciably greater ionization potential for removal of the valence electrons on Mn(II), as would be the case if strong field ligands such as oxo(hydroxo) and carboxylato are replaced by weak field ligands such as hydroxo(aqua) and histidine, respectively. The higher ionization potential would reflect weaker electron repulsion from the surrounding ligands and hence also a correspondingly smaller degree of spin exchange onto the ligands which is the source of exchange coupling (Hay et al., 1975). This mechanism would be sensitive to the chemical identity of all the ligands, not just the bridging ligands. Accordingly, the proposed difference in the degree of protonation of the bridging aqua/hydroxo ligands of arginase vs MnCat is not the only possible interpretation of the Heisenberg exchange data. The structural origin of the transformation of the ZFS of arginase by borate binding to the active site remains to be supported by a systematic examination of additional inhibitors. Accordingly, the structural model in Figure 9B should be considered preliminary.

NOTE ADDED IN PROOF

Chloride inhibition of catalase activity has recently revealed two inhibition constants of 0.25 mM and 100–250 mM (Shank, 1994).

ACKNOWLEDGMENT

We thank Professor Tad Day for helpful discussions.

SUPPLEMENTARY MATERIAL AVAILABLE

Four figures illustrating, for compounds 2, 3, and MnCat-(II,II)Cl, the temperature dependence of the EPR line shape, fits of the EPR intensity vs temperature to the Boltzmann populations predicted for the HDVV exchange energy levels,

and deconvolution of the spectra into triplet and quintet state spectra (11 pages). Ordering information is given on any current masthead page.

REFERENCES

- Antanaitis, B. C., Brown, R. D., III, Chasteen, N. D., Freedman, J. H., Koenig, S. H., Lillenthal, H. R., Peisach, J., & Brewer, C. F. (1987) *Biochemistry* 26, 7932–7937.
- Baranowski, J., Cukierda, T., Jezowska-Trzebiatowska, B., & Kozłowski, H. (1979) *J. Magn. Reson.* 33, 585–593.
- Barynin, V. V. (1991) *J. Inorg. Biochem.* 43, 362.
- Barynin, V. V., & Grebenko, A. I. (1986) *Dokl. Akad. Nauk SSSR* 286, 461–464.
- Barynin, V. V., Vagin, A. A., Melik-Adamyan, V. R., Grebenko, A. I., Khangulov, S. V., Popov, A. N., Andrianova, M. E., & Vainshtein, B. K. (1986) *Dokl. Akad. Nauk SSSR* 288, 877–880 (Russian).
- Beyer, W. F., & Fridovich, I. (1985) *Biochemistry* 24, 6460–6467.
- Bossek, U., & Wieghardt, K. (1989) *Inorg. Chim. Acta* 165, 123–129.
- Cammack, R., Chapmann, A., Lu, W.-P., Karagouni, A. A., & Kelly, D. P. (1989) *FEBS Lett.* 252, 239–243.
- Caneschi, A., Ferraro, F., Gatteschi, D., Chiaro Melandui, M., Rey, P., & Sessoli, R. (1989) *Angew. Chem., Int. Ed. Engl.* 28, 1365.
- Carrel, H. L., Glusker, J. P., Burger, V., Manfre, F., Tritsch, D., & Biellmann, J.-F. (1989) *Proc. Natl. Acad. Sci. U.S.A.* 86, 4440.
- Chang, H.-R., Larsen, S. K., Boyd, P. D. W., Pierpont, C. G., & Hendrickson, D. N. (1988) *J. Am. Chem. Soc.* 110, 4565–4576.
- Coles, B. A., Orton, J. W., & Owen, J. (1960) *Phys. Rev. Lett.* 4, 116.
- Collyer, C. A., Henrick, K., & Blow, D. M. (1990) *J. Mol. Biol.* 212, 211–235.
- Cristmas, C., Vincent, J. B., Huffman, J. C., Christou, G., Chang, H.-R., & Hendrickson, D. N. (1987) *J. Chem. Soc., Chem. Commun.*, 236–238.
- Davies, J. F., II, Hostomka, Z., Hostomsky, Z., Jordan, S. R., & Matthews, D. A. (1991) *Science* 252, 88–95.
- DeVore, T. C., Van Zee, R. J., & Weltner, W., Jr. (1978) *J. Chem. Phys.* 68, 3522.
- Dismukes, G. C. (1993) Polynuclear Manganese Enzymes, in *Bioinorganic Catalysis* (Reedijk, J., Ed.) Marcel Dekker, Amsterdam.
- Dismukes, G. C., & Siderer, Y. (1981) *Proc. Natl. Acad. Sci. U.S.A.* 78, 274–278.
- Downard, A. J., McKee, V., & Tandon, S. (1990) *Inorg. Chim. Acta* 173, 181–190.
- Dowsing, R. D. (1970) *J. Magn. Reson.* 2, 332–337.
- Dowsing, R. D., & Gibson, J. F. (1969) *J. Chem. Phys.* 50, 294–303.
- Flassbeck, C., Weighardt, K., Bill, E., Butzlaff, Ch., Trautwein, A. X., Nuber, B., & Weiss, J. (1992) *Inorg. Chem.* 31, 21–26.
- Fronko, R. M., Penner-Hahn, J. E., & Bender, C. J. (1988) *J. Am. Chem. Soc.* 110, 7555.
- Gultneh, Y., Farooq, A., Liu, Sh., Karlin, K. D., & Zubieta, J. (1992) *Inorg. Chem.* 31, 3607–3611.
- Hardman, K. D., Agarwal, R. C., & Freiser, M. J. (1982) *J. Mol. Biol.* 157, 69–86.
- Harris, E. A. (1972) *J. Phys. C5*, 338.
- Harris, E. A., & Owen, J. (1963) *Phys. Rev. Lett.* 11, 9.
- Hay, P. J., Thibault, J. C., & Hoffmann, R. (1975) *J. Am. Chem. Soc.* 97, 4884–4899.
- Heming, M., Lehmann, G., Mosebach, H., & Siegel, E. (1982) *Solid State Commun.* 44, 543–546.
- Hodgson, D. J., Schwartz, B. J., & Sorrell, T. N. (1989) *Inorg. Chem.* 28, 2226–2228.
- Kessissoglou, D. P., Butler, W. M., & Pecoraro, V. L. (1987) *Inorg. Chem.* 26, 495–503.
- Khangulov, S. V., Barynin, V. V., Melik-Adamyan, V. R., Grebenko, A. I., Voevodskaya, N. V., Blumenfeld, L. A., Dobryakov, S. N., & Il'yasova, V. B. (1986) *Bioorg. Khim.* 12, 741–748 (Russian).
- Khangulov, S. V., Voevodskaya, N. V., Barynin, V. V., Grebenko, A. I., & Melik-Adamyan, V. R. (1987) *Biofizika* 32, 960–966 (Russian).

- Khangulov, S. V., Andreeva, N. E., Gerasimenko, V. V., Goldfeld, M. G., Barynin, V. V., & Grebenko, A. I. (1990a) *Russ. J. Phys. Chem.* **64**, 10–16.
- Khangulov, S. V., Barynin, V. V., Voevodskaya, N. V., & Grebenko, A. I. (1990b) *Biochim. Biophys. Acta* **1020**, 305–310.
- Khangulov, S. V., Barynin, V. V., & Antonyuk-Barynina, S. V. (1990c) *Biochim. Biophys. Acta* **1020**, 25–33.
- Khangulov, S. V., Goldfeld, M. G., Gerasimenko, V. V., Andreeva, N. E., Barynin, V. V., & Grebenko, A. I. (1990d) *J. Inorg. Biochem.* **40**, 279–292.
- Khangulov, S., Sivaraja, M., Barynin, V. V., & Dismukes G. C. (1993) *Biochemistry* **32**, 4912–4924.
- Kitajima, N., Singh, U. P., Amagai, H., Osawa, M., & Moro-oka, Y. (1991a) *J. Am. Chem. Soc.* **113**, 7757–7758.
- Kitajima, N., Osawa, M., Tanaka, M., & Moro-oka, Y. (1991b) *J. Am. Chem. Soc.* **113**, 8952–8953.
- Kono, Y., & Fridovich, I. (1983a) *J. Biol. Chem.* **258**, 6015–6019.
- Kono, Y., & Fridovich, I. (1983b) *J. Biol. Chem.* **258**, 13646–13648.
- Lambert, S. L., & Hendrickson, D. N. (1979) *Inorg. Chem.* **18**, 2683–2686.
- Mabad, B., Tuchagues, J.-P., Hwang, Y. T., & Hendrickson, D. N. (1985) *J. Am. Chem. Soc.* **107**, 2801–2802.
- Mabad, B., Cassoux, P., Tuchagues, J.-P., & Hendrickson, D. N. (1986) *Inorg. Chem.* **25**, 1420–1431.
- Mathur, P., Crowder, M., & Dismukes, G. C. (1987) *J. Am. Chem. Soc.* **109**, 5227–5233.
- Meirovitch, E., Luz, Z., & Kalb (Gilboa), A. J. (1974) *J. Am. Chem. Soc.* **96**, 7538–7546.
- Menage, S. (1988) Ph.D. Thesis, University of Paris Sud (Orsay).
- Mikuriya, M., Kawasaki, Y., Tokii, T., Yanai, S., & Kawamori, A. (1989) *Inorg. Chim. Acta* **156**, 21–22.
- Mikuriya, M., Adachi, F., Iwasawa, H., Handa, M., Koikawa, M., & Okawa, H. (1991) *Inorg. Chim. Acta* **179**, 3–5.
- Moriya, T. (1960) *Phys. Rev.* **120**, 91–98.
- Nishida, Y. (1987) *Chem. Lett.* 2151–2152.
- Nishida, Y., Oshino, N., & Tokii, T. (1988) *Z. Naturforsch. B43*, 472.
- Owen, J., & Harris, E. A. (1972) *Electron Paramagnetic Resonance* (Geschwind, S., Ed.) pp 427–492, Plenum Press, New York.
- Penner-Hahn, J. E. (1992) in *Manganese Redox Enzymes* (Pecoraro, V. L., Ed.) pp 29–45, Verlag Chemie, New York.
- Pessiki, P. J., & Dismukes, G. C. (1994) *J. Am. Chem. Soc.* **116**, 898–903.
- Pessiki, P. J., Khangulov, S. V., Dismukes, G. C., & Barynin, V. V. (1992) in *Macromolecular Host-Guest Complexes: Optical, Optoelectronic and Photorefractive Properties and Applications* (Jenheke, S., Ed.) Materials Vol. 277, pp 75–86, Res. Soc., Pittsburgh, PA.
- Pessiki, P. J., Khangulov, S. V., Ho, D. M., & Dismukes, G. C. (1994) *J. Am. Chem. Soc.* **116**, 891–897.
- Que, L., Jr., & True, A. E. (1990) *Prog. Inorg. Chem.* **38**, pp 97–200.
- Reczkowski, R. S. (1990) Ph.D. dissertation, Characterization of the Kinetic and Catalytic Mechanism of Rat Liver Arginase, Temple University, Philadelphia, PA.
- Reczkowski, R. S., & Ash, D. E. (1992) *J. Am. Chem. Soc.* **114**, 10992–10994.
- Sakiyama, H., Tamaki, H., Kodera, M., Matsumoto, N., & Okawa, H. (1993) *J. Chem. Soc., Dalton Trans.*, 591–595.
- Schake, A. R., Vincent, J. B., Li, Q., Boyd, P. D. W., Folting, K., Huffman, J. C., Hendrickson, D. N., & Christou, G. (1989) *Inorg. Chem.* **28**, 1915.
- Schultz, C., Bertini, I., Viezzoli, M. S., Brown, R. D., III, Koeng, S. H., & Coleman, J. E. (1989) *Inorg. Chem.* **28**, 1490–1496.
- Shank, M. (1994) B.Sc. Thesis, Princeton University, Princeton, NJ.
- Sheats, J. E., Czernuszewicz, R. S., Dismukes, G. C., Rheingold, A. L., Petrouleas, V., Stubbe, J., Armstrong, W. H., Beer, R. H., & Lippard, S. J. (1987) *J. Am. Chem. Soc.* **109**, 1435–1444.
- Smith, T. D., & Pilbrow, J. R. (1974) *Coord. Chem. Rev.* **13**, 173–278.
- Suzuki, M., Mikuria, M., Murata, S., Uehara, A., Oshio, H., Kida, S., & Saito, K. (1987a) *Bull. Chem. Jpn.* **60**, 4305–4312.
- Suzuki, M., Murata, S., Uehara, A., Kida, S., & Saito, K. (1987b) *Chem. Lett.*, 281–284.
- Vainshtein, B. K., Melik-Adamyan, V. R., Barynin, V. V., & Vagin, A. A. (1984) in *Progress in Bioorganic Chemistry and Molecular Biology* (Ovchinnikov, Yu., Ed.) pp 117–132, Elsevier Scientific Publishing, Amsterdam, London, and New York.
- Vainshtein, B. K., Melik-Adamyan, V. R., Barynin, V. V., Vagin, A. A., & Grebenko, A. I. (1985) *Proc. Int. Symp. Biomol. Struct. Interactions, Suppl. J. Biosci.* **8**, 471–479.
- Van Zee, R. J., & Weltner, W., Jr. (1981) *J. Chem. Phys.* **74**, 4330.
- Van Zee, R. J., DeVore, T. C., & Weltner, W., Jr. (1979) *J. Chem. Phys.* **71**, 2051.
- Waldo, G. S., Yu, S., & Penner-Hahn, J. E. (1992) *J. Am. Chem. Soc.* **114**, 5869–5870.
- Wasserman, E., Snyder, L. C., & Yager, W. A., (1964) *J. Chem. Phys.* **41**, 1763–1772.
- Weighardt, K., Bossek, U., Bonvoisin, J., Beauvillain, P., Girerd, J. J., Nuber, B., Weiss, J., & Heinze, J. (1986) *Angew. Chem.* **98**, 1026.
- Weighardt, K., Bossek, U., Nuber, B., Weiss, J., Bonvoisin, J., Corbella, M., Vitols, S. E., & Girerd, J. J. (1988) *J. Am. Chem. Soc.* **110**, 7398.
- Whitlow, M., Howard, A. J., Finzel, B. C., Poulos, T. L., Winborne, E., & Gilliland, G. L. (1991) *Proteins* **9**, 153–173.
- Willing, A., Follmann, H., & Auling, G. (1988) *Eur. J. Biochem.* **170**, 603–611.
- Yu, S.-B., Wang, C.-P., Day, E. P., & Holm, R. H. (1991) *Inorg. Chem.* **30**, 4067–4074.
- Yu, S.-B., Lippard, S. J., Shweky, I., & Bino, A. (1992) *Inorg. Chem.* **31**, 3502–3504.
- Zheng, M., Khangulov, S. V., Dismukes, G. C., & Barynin, V. V. (1994) *Inorg. Chem.* **33**, 382–387.

BI942255T